

Deposit Morphology and Head Loss Development in Porous Media

SRINIVAS VEERAPANENI[†] AND
MARK R. WIESNER^{*‡}

*Department of Environmental Science and Engineering
(MS 317), George R. Brown School of Engineering, Rice
University, 6100 Main Street, Houston, Texas 77005*

Experimental observations of monodispersed latex particles filtered through a bed of spherical glass beads indicated that flow rate plays an important role in head loss development by influencing the morphology of the deposits as well as the deposit distribution along the depth of the bed. The distribution of the deposits along the depth of porous media was more uniform at higher velocities. Deposits formed at low filtration (Darcy) velocities produced higher specific head loss (head loss per unit particle mass deposited) compared to the deposits formed at higher velocities. The fractal dimensions of the deposits formed in the porous medium varied with filtration velocity. The fractal dimensions of the deposits increased with increase in velocity at either end of the range of flow rate (0.002–0.4 cm/s) investigated. This is consistent with the low specific head losses observed at higher superficial velocities and with the theory of increasing fractal dimension as particle transport becomes more ballistic. The low fractal dimensions observed in the intermediate velocities (0.04 to approximately 0.15 cm/s) appear to be due to the formation of compact columnar structures. This conclusion was supported by Monte-Carlo simulations of colloid deposition from 2-D stagnation flow which were performed to approximate particle deposition at the top of filter grains.

Introduction

The premise of this work is that the morphology of particle deposits may significantly affect the flow and mass transport characteristics of many natural and engineered porous media such as packed bed filters, membrane filters, ground water aquifers, delivery systems for ground water bioremediation, and aquifer recharge wells. As a suspension of particles flows through a porous medium, some of the particles, through a number of possible transport and attachment mechanisms, deposit on the immobile phase of the porous medium. The deposited particles themselves become sites for subsequent particle deposition, thereby increasing the particle retention efficiency of the bed (usually referred to as the “ripening” stage of the filter bed). As particles are removed, the geometry and the structure of the medium and the surface characteristics of the porous medium change over time, influencing subsequent particle deposition and fluid flow. The growing immobile solid phase comprising the initial porous medium and the retained particles causes higher drag on the fluid, resulting in higher head loss across the bed. As pores in the porous bed become clogged, interstitial velocity and shear

stresses increase, possibly resulting in reduced rates of deposition and even reentrainment of the deposited particles which may redeposit downflow in the porous medium. The morphology of the particle deposits will likely play a role in their potential for reentrainment. In addition, the morphology of the particle deposits may significantly influence the subsequent fluid flow and particle deposition in the porous media. For instance, like colloidal aggregates, the morphology of the colloidal deposits may affect the degree to which fluid flows around rather than through a deposit (I) and therefore determines the degree to which deposited particle surface area is exposed to fluid flow, and hence its contribution to the total drag loss in the bed. In addition, the arrangement of particles within a deposit can produce a shadowing effect in which some of the deposition sites are blocked by upstream particles. The extent of this shadowing depends on the morphology of the deposit. In this work, we examine the hypothesis that the morphology of colloidal deposits in porous media can be predicted in part as a function of the transport characteristics of particles in suspension. The relationship between deposit morphology and physical–chemical processes that form the deposit is explored experimentally and interpreted within the context of trends observed in numerical simulations of particle deposition.

Background

Simulations of particle deposition under highly idealized conditions suggest that when particle trajectories up to a deposition event are random (diffusion-limited deposition, DLD) open, dendritic deposits are formed. In contrast, particles under the influence of advective forces follow ballistic depositional trajectories (ballistic deposition, BD) and may favor more compact deposits with uniform porosity (2–8). The trends observed in deposition simulations mirror those observed in particle aggregation. Several numerical (9–11) and experimental (12–16) studies involving colloidal aggregation under various dominant transport mechanisms have indicated that the structure of an aggregate appears to depend on the dominant physical and chemical mechanisms that cause aggregation. For example, when diffusive transport is the dominant aggregation mechanism (diffusion-limited aggregation, DLA), aggregates tend to be more open and less compact compared to the compact structures produced when particles follow ballistic trajectories before adhesion occurs (ballistic aggregation, BA).

The morphology of colloidal aggregates and deposits may be geometrically complex. Attempts to relate characteristics of aggregates such as density, size, or porosity to the conditions in which aggregates are formed have led to myriad relationships, often following power laws. More consistent trends in aggregate characterization became apparent when data are interpreted in the context of fractal geometry (17–19) to describe non-integer dimensionality of complex geometrical objects. Fractal geometry allows the characterization of objects in terms of their self-similar (scale-invariant) properties (i.e., parts of the object are similar to the whole after appropriate rescaling). This property results in power-law relationships between length scales and properties such as mass, density, and surface area. For example, the mass M of a fractal object such as an aggregate is related to its size R as $M(R) \propto R^D$ where D is the fractal dimension of the aggregate. Deposits (or aggregates) formed under defined sets of transport and deposition (or aggregation) rules are consistently described by one or more fractal dimensions. Several so-called “universality classes” have been identified in which the set of transport rules correspond to a given morphology and hence fractal dimension. For instance,

* Corresponding author.

[†] Postdoctoral research associate. Telephone: (713) 527-4952 x2404. Fax: (713) 285-5203. E-mail: vasu@rice.edu.

[‡] Professor. Voice: (713) 285-5129. E-mail: wiesner@rice.edu.

Meakin (2) calculated the fractal dimension of the open structured diffusion-limited deposits to be 1.76 in 2-dimensions and 2.5 in 3-dimensions. On the contrary, simulated ballistic deposits (5–7) that are compact and uniform in structure (in terms of porosity) are characterized by fractal dimensions equal to their Euclidean dimensions. These universality classes represent idealized extreme cases that may bracket every day experience.

We have reported simulations (8) that suggest that a continuous range of deposit morphologies are formed as a function of fluid velocity and particle size. The relative diffusive or ballistic nature of a particle's trajectory can be summarized by a particle Peclet number expressing the ratio of advective (ballistic) to diffusive (random) motion. We have extended this concept to consider the ratio of all ballistic transport components of a particle's trajectory (e.g., movement in response to gravity or an applied electrical field) to random components such as Brownian or turbulent diffusion. Smaller particles in low velocity laminar flows (characterized by low Peclet numbers) follow relatively more diffusive paths, resulting in highly porous structures. Larger particles or higher fluid velocities (high Peclet numbers) tend to favor more ballistic trajectories, leading to compact deposits. In the intermediate values of Peclet number, the deposit morphology is highly sensitive to changes in fluid velocity and particle size.

Based on these results, we present the hypothesis that the morphology of colloidal deposits in porous media and its subsequent effect on particle removal and head loss development can be predicted to a useful approximation from the dominant particle transport mechanisms leading to deposition. In this paper, we present results from experiments of particle deposition in porous media designed to test the notion that under conditions of favorable deposition (no energy barrier to particle attachment) the morphology of the particle deposits can be predicted from transport-determining parameters such as particle size and filtration (Darcy) velocity. We show that the morphology of the colloidal deposits has an enormous effect on the head loss produced by a given mass of particles deposited in a porous medium.

Experimental Procedures

Materials and Methods. The experimental apparatus employed in this work is similar to that used in previous work (20) and is briefly described here. The experimental design was chosen to closely approximate the assumptions that are commonly made in modeling filtration processes (for example, spherical monodisperse particles and filter media and favorable chemical conditions). Suspensions of particles were introduced to a packed bed (filter) of porous medium. Spherical glass beads (Potters Industries Inc., Hasbrouck Heights, NJ) of sizes between 40 and 50 U.S. Standard Sieves with an average diameter of 358 μm were used as the filter media. As discussed above, the morphology of Brownian particle (diameter less than 1 μm) deposits is most susceptible to changes in physical–chemical conditions under which the deposits are formed. Moreover, the light scattering technique used to determine fractal dimensions requires that particles be small relative to the wavelength λ of the incident light source (Helium-Neon laser; $\lambda = 632.8 \text{ nm}$). Hence, all experiments were conducted with suspensions of spherical monodispersed polystyrene latex particles of size 69 nm (Seradyn Inc., Indianapolis, IN). The filter column was fabricated from a 2.5 cm inside diameter cast plexiglass tube. A constant and nearly pulse-free flow through the filter bed was provided by a magnetic-drive gear pump (Ismatic variable speed pump drive and Micropump pump head; Cole Parmer Instrument Co., Chicago, IL). Latex particles were injected into the main flow just above the column using a syringe pump (Harward Apparatus Inc., South Natick, MA). Calcium nitrate at a concentration of 0.1 M was used in the feed water

to destabilize the negatively charged latex particles. The pH was maintained close to 7 using $5 \times 10^{-5} \text{ M NaHCO}_3$. These chemical conditions were determined based on results from jar tests conducted with varying concentrations of calcium nitrate at constant ionic strength (ionic strength was adjusted using sodium nitrate as a background electrolyte). The electrophoretic mobilities of the influent latex particles in all the experiments under these chemical conditions were low (Table 1). Deionized and degassed Milli-Q water was used, and all chemicals were of reagent grade. All solutions were filtered through a 0.22 μm membrane 3 times. A data acquisition system was used to monitor pressure continuously through three sampling ports with transducers (IC Sensors, Milpitas, CA). Two pressure ports were located just above and below the bed, while one was located at an intermediate depth below the top surface of the bed. The analog signal from the transducers was converted to a digital signal for acquisition on a Macintosh computer using a commercial hardware and software package (Biopac Systems, Goleta, CA). The sampling interval varied with the duration of the experiments from 10 s for 2 h long experiments to 5 min for experiments longer than 24 h. The influent and effluent concentrations of particles were determined by absorbance on a spectrophotometer (Hitachi U-2000 Double-Beam UV/Vis spectrophotometer) at a wavelength of 262 nm, based on the stock suspension concentrations as reported by the manufacturer (10% by volume). A good linear relationship ($r^2 > 0.991$) between the absorbance of influent solutions of different experiments and the particle concentrations was observed. The zeta potential and electrophoretic mobility of latex particles were measured by laser light scattering, using a Malvern Zetasizer IIc (Malvern Instruments Ltd., Wordestershire, England).

Typical Experimental Procedure. The required mass of glass beads, determined from the estimated porosity and the desired depth of porous medium, was immersed overnight in an electrolyte solution of the same concentration as that utilized to destabilize latex particles. Before each experiment, the glass beads were rinsed with fresh electrolyte solution 5 times. The column was filled with the same electrolyte solution and packed up to the lower pressure port with 6 mm diameter glass beads. A Teflon screen of pore size 297 μm and thickness 410 μm was used to separate the large support glass beads from the smaller filter media. The small glass beads were dropped into the column using a funnel and spoon, and the column was constantly tapped to ensure proper packing. About 3 L of particle-free influent solution was passed through the column at 200 mL/min flow rate to ensure maximum compaction of the packed bed. Head loss across the bed was then measured with varying flow rates and was compared with predictions based on the Kozeny–Carman model (21, 22). Conformity to the Kozeny–Carman equation was used as a check on the preparation of the filter column before each experiment. The latex solution was then loaded into two syringes (Monoject, polypropylene, 140 mL capacity) and mounted on a syringe pump. Feed to the packed bed was directed away from the column using a 3-way valve, and the syringe pump was switched on. After 10 min, several samples were taken, and the influent particle concentration was measured to verify that the desired concentration of particles in the feed was obtained. The data acquisition system for monitoring pressure was then initiated, and flow was redirected to the packed bed. Effluent samples were collected at appropriate intervals, as determined from tracer studies, and analyzed within a minute of collection. The physical and chemical conditions of the experiments are listed in Table 1.

At the end of each experiment, the column was disconnected from pumps and pressure transducers, and the particle deposits were chemically fixed to allow for their removal from the porous medium. The top section of the column was

TABLE 1. Physical and Chemical Conditions of Influent Bed Depth $L = 2$ cm; Suspended Particle Diameter (d_p) = 0.069 μm ; Filter Grain Diameter (d_c) = 358 μm

expt no.	influent particle concn, C_0 (mg/L)	superficial velocity, μ_s (cm/s)	zeta potential of influent particles, ζ_p (mV)	electrophoretic mobility of influent particles, ($\mu\text{m s}^{-1} \text{V}^{-1} \text{cm}^{-1}$)	pH	T ($^{\circ}\text{C}$)
61	16.3	3.528E-2	-4.84	-0.41	6.85	20.6
62	4.14	1.351E-1	<i>a</i>	<i>a</i>	6.61	21.1
63	5.49	2.716E-1	-5.14	-0.39	6.77	21.7
64	16.15	1.385E-1	-4.83	-0.68	6.65	23.8
65	16.15	3.115E-1	-3.16	-0.48	6.75	23.8
66	8.234	1.371E-1	-5.65	-0.56	6.63	23.6
67	94.1	2.450E-3	-7.34	-0.44	6.5	21
68	5.0	7.322E-3	-2.23	-0.58	6.68	22
69	26.367	5.112E-1	-6.64	-0.35	6.71	22.6
70	4.06	1.664E-2	<i>a</i>	<i>a</i>	6.92	22.5
71	6.3	6.956E-2	-3.29	-0.52	6.68	23.2
72	7.35	2.044E-1	-6.32	-0.34	6.66	23.2
73	20.32	2.064E-1	-6.9	-0.51	6.71	23.7
74	18.1	2.558E-1	-4.42	-0.62	6.82	23.1
75	7.25	1.688E-1	-6.38	-0.37	6.73	24.2
76	10	2.330E-1	-6.72	-0.47	6.47	23.9
83	7.25	1.688E-1	-5.81	-0.56	6.5	21.3
84	7.25	1.688E-1	-5.64	-0.47	6.46	22.6
85	46.2	1.331E-3	-4.06	-0.56	6.61	22.3
86	2.988	5.053E-2	-6.63	-0.5	6.9	22.2
87	4.94	1.018E-1	-6.13	-0.35	6.81	21.8
88	7.34	1.028E-1	-6.06	-0.12	6.53	22.5
89	9.74	1.038E-1	-3.56	-0.47	6.59	21.6
90	15.096	1.062E-1	-5.42	-0.59	6.33	21.8
91	12.31	2.230E-1	-6.47	-0.32	6.87	22.3
92	3.38	5.991E-3	<i>a</i>	<i>a</i>	6.7	22.1
93	2.868	1.498E-2	<i>a</i>	<i>a</i>	6.8	22.3
94	2.437	1.897E-2	<i>a</i>	<i>a</i>	6.7	22.2
95	4.826	1.043E-1	-4.23	-0.56	6.68	22.4
96	3.315	3.388E-2	<i>a</i>	<i>a</i>	6.72	22.4
97	3.9	4.993E-2	<i>a</i>	<i>a</i>	6.6	22.3
98	3.834	4.993E-2	<i>a</i>	<i>a</i>	6.7	22.4
99	0.88397	6.354E-3	<i>a</i>	<i>a</i>	6.81	22.5
100	27.27	2.929E-1	-4.18	-0.62	6.7	21.8
101	10.0	2.796E-1	-5.62	-0.397	6.8	22.2
102	21.0	3.328E-1	-4.75	-0.68	6.68	22.4

^a Could not measure because of low concentrations of particles.

removed, and the feed solution in the head space above the porous media containing particles was gently removed using a syringe. A 12 g/L solution of bovine albumin solution (Sigma Chemical Co., St. Louis, MO) was then gently added along the walls of the column using a syringe fitted with a series of filters (1.2 μm , 0.8 μm , 0.45 μm , and 0.22 μm in pore size). After the head space was filled up with albumin solution, the effluent valve at the bottom of the column was opened, and as the protein solution dripped out of the column under gravity, more was added at the top. After approximately 100 cm^3 of the protein solution was passed through the column, the effluent valve was closed, and the column was left undisturbed for 1 h to allow adsorption of protein onto latex particle surfaces. At the end of 1 h, the same procedure was repeated with a 10% solution of formaldehyde. Formaldehyde reacts with the amino acids, resulting in cross-linking of proteins, thereby adding stability to the morphology of the deposits. Treatment with formaldehyde is a commonly used technique to preserve structural features of cell tissues and isolated protein preparations for subsequent microscopic examination. After the filter bed was soaked in 10% formaldehyde for 1 h, the column was tilted into a beaker consisting of 10% formaldehyde solution, until the filter media gently slid into the beaker. Before this was attempted, it was made sure that the head space in the column was filled with the same solution, and while the column was tilted into the beaker, care was taken to ensure that the packed bed was always in contact with the solution. In most experiments, especially those conducted at high flow rates, the filter bed moved as a solid body through the filter column, and as it slid into the

beaker, it broke up, with the glass beads settling to the bottom of the beaker, leaving latex particle deposits suspended in solution. In some very low flow rate experiments, the top section of the filter bed (less than 1 cm deep) would not break and needed gentle prodding with a Teflon rod before breaking up. The deposits were then transferred into a Burchard cell for light scattering measurements.

Light Scattering Measurements on Deposits. Static light scattering experiments were performed to measure the angular dependence of intensity of light [$I(q)$] scattered by colloidal deposits which were dislodged from the porous medium after each experiment. Here q , the scattering wave number, is the modulus of the scattering vector, defined as $q = 4\pi n\lambda^{-1} \sin(\theta/2)$, where n is the refractive index of the solvent, λ is the wavelength of the incident beam, and θ is the scattering angle. In these experiments, the length scales over which the deposits are probed depend on the wavelength of the light source and angle as q^{-1} . Using the radii of cluster (R_c) and primary particles (a_p) as reference length scales, the fractal dimension, D , of the clusters can be obtained from a log-log plot of the scattering intensity [$I(q)$] versus the scattering wave number (q) as follows (13, 23-26):

$$I(q) \propto q^{-D} \text{ for } qR_c \gg 1 \text{ and } qa_p \ll 1 \quad (1)$$

Light scattering was measured using a Malvern 4700c system (Malvern Instruments Ltd.) comprised of a variable-angle light scattering spectrometer (PCS100) interfaced to a K7032 computer correlator. The goniometer of the PCS100

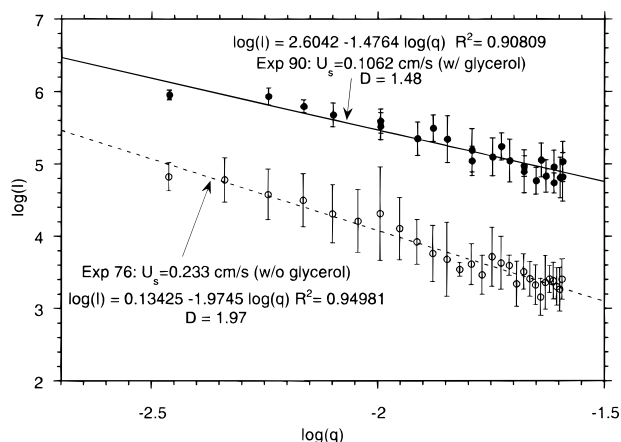


FIGURE 1. Double logarithmic plot of $I(q)$ vs q .

allowed the photomultiplier detector to be set to any scattering angle between 10° and 150° with respect to the incident laser beam within an accuracy of 0.01° . The light source was provided by a 30 mW vertically polarized (i.e., perpendicular to the scattering plane) helium–neon laser (wavelength = 632.8 nm; Siemens Model LGK7626S) operating in a single mode (TEM $_{00}$). The Burchard cell containing the deposits was placed at the center of the goniometer, immersed in a vat of clean water (filtered through a $0.22 \mu\text{m}$ filter 3 times) that served to couple the thermostat system to the sample, maintaining the temperature at $25 \pm 1^\circ\text{C}$. The alignment of the instrument was verified by measuring the intensity of light scattered by toluene at different angles, and the deviation around the mean was found to be $<1\%$ for most of the range, as is expected of Rayleigh scatterers. The stepping motor control of the goniometer allowed measurement of scattered light intensity over a range of angles at fixed intervals. At each angle, the intensity was recorded for a specified length of time and translated via the optical normalization (which corrects for the changing in viewing volume in the cell as a function of angle) required to a relative intensity value. Scattered intensity was measured over an angular range of 10° to 150° . In all the experiments, the dislodged deposits were clearly visible with diameters larger than 1 mm.

Light scattering measurements were performed on an average of 10 samples from each experiment and at least 5 times on each sample. In earlier experiments, significant settling of the deposits in the sample cell was observed as the goniometer traversed the full range of angles. To make the deposits more buoyant, glycerol solution was used in later experiments as the suspending medium for the deposits. After the deposit was soaked with formaldehyde for 1 h, the same procedure as was followed for protein and formaldehyde solutions was repeated with a 32.2% by weight glycerol solution. This concentration of glycerol solution was found, by trial and error, to be ideal to avoid any significant settling of deposits during light scattering measurements.

In Figure 1, the variation of scattered light intensity, $I(q)$, as a function of scattering wave number (q) is plotted on a double logarithmic plot for two typical experiments. The differences in intercepts are due to the differences in concentrations of deposits in the sample cell (the total deposited particle mass varied between experiments). The negative of the slope of the linear fit between $\log [I(q)]$ and $\log (q)$ gives the fractal dimension (eq 1). Deposits formed at a superficial velocity of 0.106 cm/s have a fractal dimension of 1.48, while those formed at 0.233 cm/s have a fractal dimension of 1.97. In experiment 90, the deposits were suspended in glycerol during light scattering measurements. The use of glycerol to suspend the deposits during light scattering measurements appears to have reduced the variance in the measurements (Figure 1). However, despite the

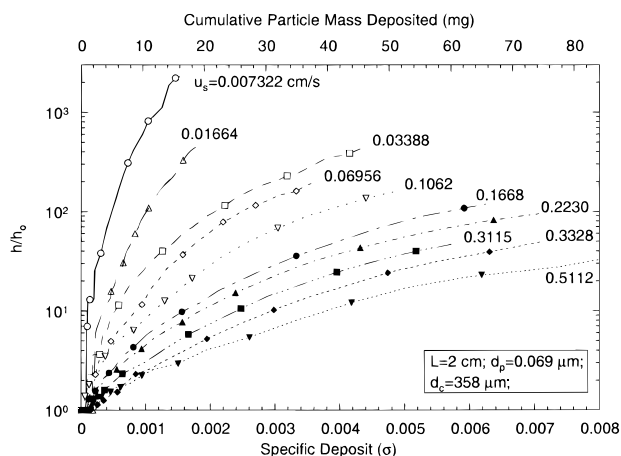


FIGURE 2. Head loss increase as a function of specific deposit during filtration of 69 nm particles at different superficial velocities.

precautions described, several limitations of the procedure could not be completely resolved and may have contributed to the variance in the results: (i) The light scattering measurements were performed on the deposits at the end of an experiment. The “stage” at which the experiment ended could not be determined. For instance, some experiments may have ended before significant restructuring/break-up of the deposits occurred during the course of the filtration and some after or during the restructuring process. These potential differences complicate comparison of fractal dimensions. (ii) Since all the deposits in the filter bed were removed at one time (i.e., at the end of the experiment), the light scattering measurements reflect the scattering properties of all the deposits formed at different depths of the bed. (iii) The procedure of “chemical fixing” the deposits using protein and formaldehyde treatment as described above was found to yield satisfactory results for trial aggregates formed in the diffusion-limited aggregation regime. Nonetheless, there is always a possibility of break-up and/or rearrangement of the deposits during transfer from the bed to the sample cell.

Results and Discussion

Effect of Flow Rate on Head Loss Development across the Filter Bed. Increases in head loss over the entire bed depth (2 cm) as a function of specific deposit, σ , (defined as volume of particles deposited per unit volume of bed), during the filtration of 69 nm particles at different superficial velocities are compared in Figure 2. For clarity, results are presented on semi-log axes. The data show a clear trend: for the same particle mass deposited, conditions that favor ballistic transport (higher superficial velocities in these experiments) result in less head loss per unit particle mass deposited. Steep increases in head loss were observed at very low superficial velocities ($u_s < 0.07$ cm/s). At higher superficial velocities, the increase in head loss was more gradual as more particle mass deposited.

Changes in specific head loss as a function of flow rate result from two interrelated effects: the local morphology of the deposits and the distribution of deposited material with depth through the column. At low velocities or for small particles, particle transport has a relatively larger diffusive component resulting in more porous deposits. At higher velocities or for large particles, the trajectories of particles are more ballistic, and the deposits formed are more compact. Hence, for the same particle mass deposited, deposits formed at lower fluid velocities occupy more pore space in the filter bed, causing the fluid to experience more drag loss, thereby resulting in higher head losses.

The superficial velocity also affects the deposit distribution along the depth of the bed. The low removal efficiency of the packed beds at higher velocities causes particles to penetrate

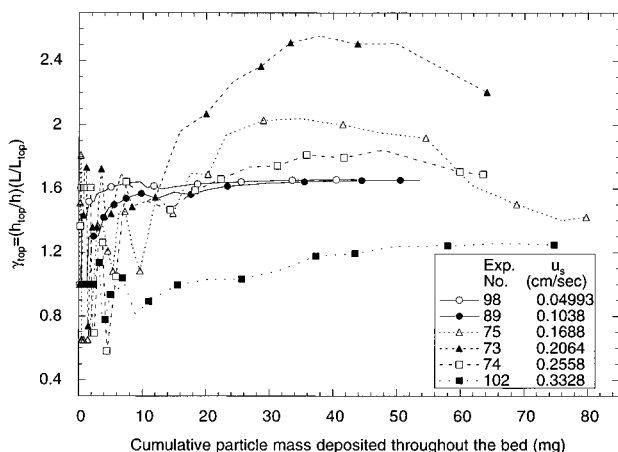


FIGURE 3. Ratio of head loss per unit depth in the top layer to that of the whole bed as a function of retained particle mass at several superficial velocities. ($h_{top} = 0.6$ cm for experiments 73, 74, and 75; $h_{top} = 1.2$ cm for experiments 89, 98, and 102).

deeper into the bed, resulting in a more homogeneous distribution of the deposits along the depth of the bed. At low velocities, the high efficiency of the packed bed may limit particle penetration to the top layers of the bed, causing rapid clogging of pores and hence higher increases in specific head loss. Conditions favoring the formation of a more porous deposit would enhance this tendency for material to accumulate at the top of the packed bed.

To better isolate the effect of deposit morphology on head loss development from that of deposit distribution along the depth of the bed, experiments were run on shallow beds of 2 cm depth. Even at this shallow depth, it was observed that deposition was not uniform over the entire depth of the bed, especially at low superficial velocities. At a superficial velocity of 0.0505 cm/s, a distinct white band was observed in the top 0.6 cm of bed, suggesting that this region retained significantly more particles than the rest of the bed (the latex particles are milky white in color). At higher velocities (0.1062 and 0.1688 cm/s), the depth of this white band was higher (0.8 and 1 cm, respectively). At a still higher velocity of 0.223 cm/s, the whole bed had a light whitish color with the top 1.5 cm being slightly whiter than the rest of the bed. At velocities higher than 0.22 cm/s, the color of the bed was more uniform, although a slight gradation along the depth of the bed was still evident, suggesting that the deposits might be more uniformly distributed with depth. The relative removal of particles by the different sections of the bed was not quantified as the particle concentration in the effluent was measured only at the bottom of the 2 cm bed. However, the head loss was measured over the entire depth of the bed, as well as at one intermediate depth [at 0.6 cm depth from the upstream end of the bed in some experiments (experiment numbers < 76), and at 1.2 cm depth in other experiments (experiment numbers ≥ 77). The head loss data in different sections of the bed give some indication of the mass distribution along the depth of the bed.

In Figure 3, the ratio of head loss per unit depth in the top section of the bed to that of whole bed, $\gamma_{top} = (h_{top}/L_{top}) / (h/L)$, is plotted as a function of total particle mass deposited for experiments run at different superficial velocities. For clarity, only data from experiments conducted at representative superficial velocities are shown. The fluctuations observed at low values of retained particle mass are due to the sensitivity of the pressure transducers. During the initial stages of filtration, the rate of particle deposition is low, and the increase in head loss is within the sensitivity of the transducers (0.02 psi). The ratio γ_{top} attains its maximum value (equal to the ratio of the length of the whole bed to that of the top section) when all the head loss occurs in the top

section of the bed. Hence in experiments with serial numbers less than 77, the maximum value of γ_{top} is 3.33 ($=2/0.6$), and for experiment numbers ≥ 77 , γ_{top} attains a maximum value at 1.67 ($=2/1.2$). At superficial velocities less than 0.11 cm/s, almost all the head loss occurred in the top section of the bed. Two examples of this ($u_s = 0.05$ and 0.1 cm/s) are shown in Figure 3. In these two experiments (98 and 89), γ_{top} quickly increases close to its maximum value of 1.67. For velocities in the range of $0.11 < u_s < 0.24$ cm/s, the ratio γ_{top} first increased and then decreased (for example, experiments 75, 73, and 74 in Figure 3). However, the value of γ_{top} is always greater than 1, indicating that the head loss in the top section is higher than that in the bottom section. In all the experiments, the head loss across the entire bed depth increased with particle mass deposited. Hence, any decline in γ_{top} indicates two (perhaps concurrent) possibilities. One possibility is that the upper section of the bed may have reached a nonretentive stage; i.e., no further particle collection would have occurred in the upper section of the bed, and further deposition occurred primarily in the lower section of the bed. This would cause the head loss across the whole bed to increase, while the head loss in the top section of the bed would remain constant and hence the ratio γ_{top} would decrease. A second possibility is that even though deposition of particles continued in the upper section of the bed, the increased shear stresses in the bed might scour deposits and carry the fragments to the lower section of the bed. At a superficial velocity of 0.2558 cm/s, γ_{top} remained more or less constant at a value of 1.7, which is far below the possible maximum value of 3.33. This indicates that even though head loss in the top section dominates, there is significant head loss in the bottom section and the top section is still retaining some particles. At a higher velocity of 0.3328 cm/s, γ_{top} is close to 1, indicating that the head loss distribution across the bed is relatively uniform, due to the high penetration of particles at this high velocity. However, the uneven distribution of deposited particle mass cannot account for the significant changes (1–2 orders of magnitude) in head loss observed at different superficial velocities (Figure 2). These results indicate that the morphology of the deposits played an important role in the evolution of the head loss profile during filtration. In the next section, the variation in the morphology of the deposits as a function of superficial velocity is discussed in terms of the fractal dimensions of the deposits.

Fractal Dimensions of Filter Deposits Formed at Different Flow Rates. The fractal dimensions of the deposits formed during the filtration of 69 nm particles at several superficial velocities are shown in Figure 4. The solid circles represent the experiments in which deposit samples were suspended in glycerol to reduce settling of deposits during light scattering measurements. The open circles represent the experiments in which no glycerol was added to the sample. The limitations of the experimental techniques described above contributed to variance in the values of fractal dimensions measured by light scattering of deposits formed during the filtration experiments. A slight reduction in the variance of fractal dimensions determined was obtained using the glycerol procedure. The fractal dimensions of the deposits varied over a range of 1.2–2.4 as a function of superficial velocity.

The mean fractal dimensions of the deposits were observed to increase slightly (from 1.6 to 1.8) as superficial velocity increased from 0.002 to 0.03 cm/s. However, variance in the measurements does not allow adequate discrimination between these values to determine if this increase is significant. As the velocity increased from 0.04 to approximately 0.15 cm/s, the fractal dimensions of the deposits decreased significantly, and then increased with superficial velocity. An increase in fractal dimension with increasing superficial velocity, as appears to be the case in the range of 0.002–0.03

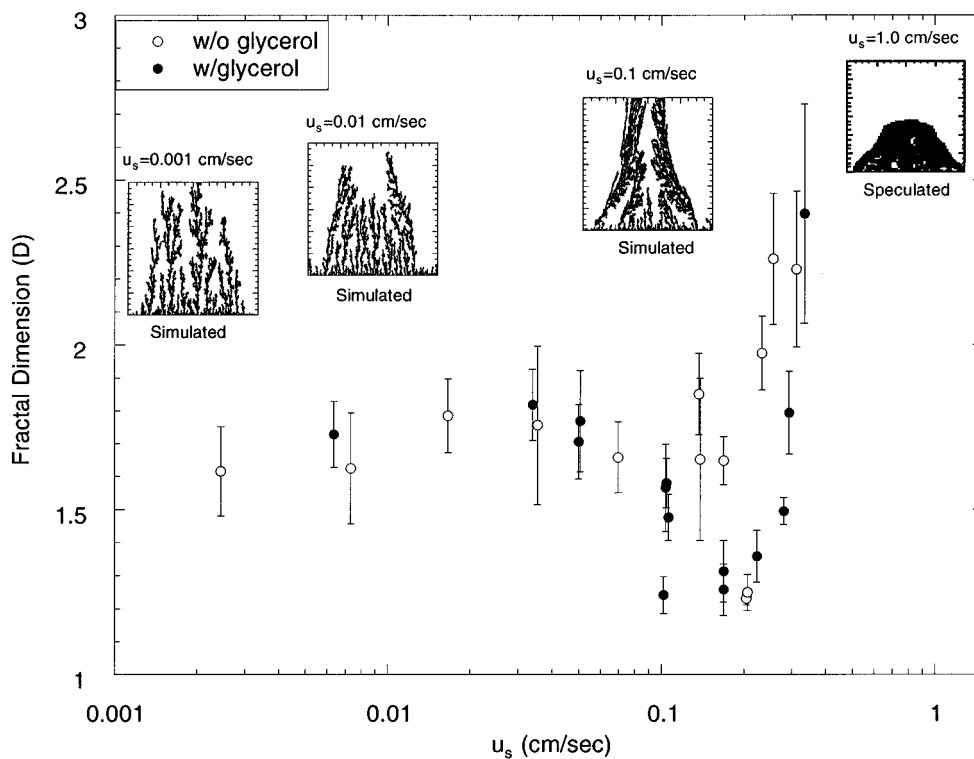


FIGURE 4. Fractal dimensions of deposits formed during filtration of 69 nm particles at different superficial velocities. Insets show results from Monte-Carlo simulations of 1 μm colloid deposition from 2-D stagnation flow.

cm/s and again at velocities greater than 0.15 cm/s, is consistent with the decrease in specific head loss (head loss per unit particle mass deposited) observed with increasing superficial velocity. This trend is also consistent with the trend anticipated from the theory of increasing fractal dimension as particle transport becomes more ballistic. The low fractal dimensions (1.2–1.4) observed in the intermediate range of fluid velocities (0.04 to approximately 0.15 cm/s) are unexpected, especially after taking into account that the specific head loss decreases with increasing superficial velocity through the whole range of flow rates investigated (Figure 2). This decline in fractal dimensions at these intermediate flow rates appears to be due to the formation of compact columnar structures. This conclusion is supported by Monte-Carlo simulations of colloid deposition from stagnation flow which were performed to approximate 2-D particle deposition at the top of the filter grains. A qualitative depiction of the evolution of deposit morphology with increasing fluid velocity, based in part on these deposition simulations, is summarized in the insets of Figure 4. Although intense CPU requirements for such simulations currently limit such simulations to particles of 1 μm or larger in diameter, a trend to form pillar-like structures as particle trajectories become more ballistic is evident (1 μm particle deposits are shown in the insets in Figure 4). At low velocities (0.001 cm/s), deposits of 1 μm particles are open dendritic structures, consistent with diffusion-limited deposition. Higher velocities (0.01 cm/s) provoke more growth of “trees” away from the stagnation point. The growth of dendrites in the deposits that are further from the stagnation point is favored over the growth of “interior” dendrites near the stagnation point. At a velocity of 0.1 cm/s, the growth of the interior dendrites is stunted, and two distinct columns develop on either side of the stagnation point. The compact linear nature of pillar-like structures produced in conditions of intermediate fluid velocity gives rise to a fractal dimension approaching 1 in the light scattering measurements. At a fluid velocity of 1.0 cm/s, simulations indicate that the two columns become more compact. Their rapid growth prevents significant deposition around the stagnation point. In reality, such formation is

unlikely to occur due to the high shear stresses at this fluid velocity. Thus, deposits formed at higher velocities are likely to be compact masses collapsed at the stagnation point (Figure 4) or wedged between pores.

To our knowledge, these are the first experimental data obtained for fractal dimensions of particle deposits in porous media. Thus, it is not strictly possible to compare these results with field observations or other experimental studies. However, there has been a significant body of data developed in filtration studies surrounding the development of head loss which can potentially be interpreted in the context of the observations reported here. In one study, Boller and Kavanaugh (27) proposed a model to calculate the increase in head loss as a function of particle mass deposited, based on the postulate that the relative density of a deposit decreases as the number of particles captured at a deposit site increases. This type of behavior is consistent with a fractal or power-law relationship between the mass of the deposit and its porosity. They empirically related the increase in head loss to the total volume of deposits (which includes the volume of particles as well as the pore volume in the deposit), and the porosity of the bed. Thus, the most important variable in their model is the pore space, which in turn depends on the number of particles deposited and the morphology of the deposit. Although they have not reported their model results in terms of fractal dimensions, we have related one of their model fitting parameters to the fractal dimension. A good fit was obtained when the fractal dimension [calculated from the values reported by them for the fitting parameters that gave best fit to the experimental results of Darby and Lawler (29)] was in the range of 2.70–2.85, suggesting that the deposits are very compact. However, they assumed that the deposits are impermeable. Since their model depends primarily on the available pore space, a good fit with experimental results is obtained only when the deposits are assumed to be very compact. Deposits with fractal dimensions less than 2.7 would quickly occupy all the pore space, and tremendous increases in head loss would be predicted by their model, as flow through the deposits was not accounted for. In another study, Hunt, Hwang, and McDowell-Boyer (28) reported

results from pilot plant filtration experiments, in which a kaolin suspension, destabilized with alum, was filtered through the sand bed. The filtration rates varied in the range 0.145–0.554 cm/s, while the influent floc size distributions were not reported. They proposed a model based on flow between two parallel plates (i.e., a pore in a filter bed) with deposited solids growing out from the walls. They further considered several deposit–porosity relationships to describe the increase in head loss, and concluded that qualitative agreement between the model and the data was observed only when the deposits were assumed to have a decreasing porosity with increasing thickness of the deposit. Again, this is consistent with a fractal deposit. They hypothesized that the flow through the porous deposits continues to filter out suspended solids (i.e., the deposits act as filter media), resulting in a decrease in porosity of the deposits.

Based on the results from this study and previous experimental results, it appears likely that in conditions typical of packed bed filters, and adsorption columns, particle deposits are likely to be compact with fractal dimensions greater than 2.5. However, in applications such as slow sand filtration and processes involving flow through aquifers, one may encounter small particles and/or very slow flow rates facilitating formation of highly open (porous) deposits which may clog the porous medium. In ground water remediation processes such as pump and treat involving ground water reinjection, higher flow rates should be preferred to prevent clogging of the aquifer with open deposits.

Acknowledgments

This material was supported in part by the Texas Higher Education Coordinating Board through the Texas Advanced Technology Program (Grant 00 3604-022) and Texas Advanced Technology Program Development (Grant 00 3604-039), U.S. Environmental Protection Agency (Cooperative Agreement CR818571-01), and U.S. Environmental Protection Agency Hazardous Substance Research Center, South/Southwest and National Science Foundation (Grant CTS-9634213). Numerical simulations reported in this work were performed in part using the Intel Touchstone Delta System operated by Caltech on behalf of the Concurrent Supercomputing Consortium (CSCC) and the parallel computer system (Paragon) operated by Caltech on behalf of the Center for Advanced Computing Research (CACR). Access to these facilities was provided by CRPC-NSF site: Rice University.

Literature Cited

- (1) Veerapaneni, S.; Wiesner, M. R. *J. Colloid Interface Sci.* **1996**, *177*, 45–57.

- (2) Meakin, P. *Phys. Rev. A* **1983**, *27*, 2616–2623.
- (3) Houi, D.; Lenormand, R. In *Kinetics of Aggregation and Gelation*; Family, F., & Landau, D. P., Eds.; North-Holland Physics Publishing: Elsevier Science Publishers B. V.: Amsterdam, 1984.
- (4) Meakin, P.; Ramanlal, P.; Sander, L. M.; Ball, R. C. *Phys. Rev. A* **1986**, *34*, 5091–5103.
- (5) Meakin, P. *J. Colloid Interface Sci.* **1985**, *105*, 240–246.
- (6) Ball, R. C.; Witten, T. A. *Phys. Rev. A* **1984**, *29*, 2966–2967.
- (7) Bensimon, D.; Shraiman, B.; Liang, S. *Phys. Lett.* **1984**, *102A*, 238–240.
- (8) Veerapaneni, S.; Wiesner, M. R. *J. Colloid Interface Sci.* **1994**, *162*, 110–122.
- (9) Jullien, R.; Botet, R.; *Aggregation and Fractal Aggregates*; World Scientific: Singapore, 1987.
- (10) Meakin, P. *Adv. Colloid Interface Sci.* **1988**, *28*, 249–331.
- (11) Meakin, P. *Annu. Rev. Phys. Chem.* **1988**, *39*, 237–267.
- (12) Lin, M. Y.; Klein, R.; Lindsay, H. M.; Weitz, D. A.; Ball, R. C.; Meakin, P. *J. Colloid Interface Sci.* **1990**, *137*, 263–280.
- (13) Lin, M. Y.; Lindsay, H. M.; Weitz, D. A.; Ball, R. C.; Klein, R.; Meakin, P. *Proc. R. Soc. London, Ser. A* **1989**, *423*, 71–87.
- (14) Pusey, P. N.; Rarity, J. G. *Mol. Phys.* **1987**, *62*, 411–418.
- (15) Wiltzius, P. *Phys. Rev. Lett.* **1987**, *58*, 710–713.
- (16) Axford, S. D. T.; Herrington, T. M. *J. Chem. Soc., Faraday Trans.* **1994**, *90*, 2085–2093.
- (17) Mandelbrot, B. B. *Les Objects Fractals: Forme, Hasard et Dimension*; Flammarion: Paris, 1975.
- (18) Mandelbrot, B. B. *Fractals: Form, Chance and Dimension*; Freeman: San Francisco, 1977.
- (19) Mandelbrot, B. B. *The Fractal Geometry of Nature*; Freeman: San Francisco, 1982.
- (20) Veerapaneni, S.; Wiesner, M. R. *J. Environ. Eng. (N.Y.)* **1993**, *119*, 172–190.
- (21) Kozeny, J. *Sitzungsber. Akad. Wiss. Wien., Abt. 2A* **1927**, *136*, 271.
- (22) Carman, P. C. *Trans. Inst. Chem. Eng.* **1937**, *15*, 150.
- (23) Kotlarchyk, M.; Chen, S.-H. *J. Chem. Phys.* **1983**, *79*, 2461–2469.
- (24) Martin, J. E.; Hurd, A. J. *J. Appl. Crystallogr.* **1987**, *20*, 61–78.
- (25) Schmidt, P. W. In *The Fractal Approach to Heterogeneous Chemistry*; Avnir, D., Ed.; John Wiley & Sons Ltd.: New York, 1989; pp 67–79.
- (26) Vicsek, T. *Fractal Growth Phenomena*; World Scientific: River Edge, NJ, 1989.
- (27) Boller, M. A.; Kavanaugh, M. C. *Water Res.* **1995**, *29*, 1139–1149.
- (28) Hunt, J. R.; Hwang, B.-C.; McDowell-Boyer, L. M. *Environ. Sci. Technol.* **1993**, *27*, 1099–1107.
- (29) Darby, J. L.; Lawler, D. F. *Environ. Sci. Technol.* **1990**, *24*, 1069–1079.

Received for review November 21, 1996. Revised manuscript received June 5, 1997. Accepted June 6, 1997.®

ES960979H

® Abstract published in *Advance ACS Abstracts*, August 1, 1997.